https://doi.org/10.15407/ujpe70.3.178

V.B. KOROVIN, I.K. TARASOV, YA.F. LELEKO,
E.L. SOROKOVYI, YU.V. KOVTUN, O.M. SHAPOVAL, M.M. KOZULYA,
O.A. LOZIN, A.M. TARASOV, E.D. KRAMS'KYI, V.V. FILIPPOV, O.V. YEVSYUKOV

National Scientific Center "Kharkiv Institute of Physics and Technology", NAS of Ukraine
(1, Akademichna Str., Kharkiv 61108, Ukraine; e-mail: korovin@kipt.kharkov.ua)

DYNAMICS OF THE UNGROUNDED ANTENNA POTENTIAL IN AN URAGAN-2M TORSATRON DURING AN RF PULSE

It has been shown that the loop radiofrequency (RF) antenna, which is used to create initial plasma in the Uragan-2M stellarator and is electrically not connected to the installation housing, acquires both negative and positive potentials during the RF pulse. The influence of the RF generator supply voltage and the working gas pressure on the antenna potential is studied. The change in the antenna potential during the simultaneous operation of two RF generators is shown. The influence of the ponderomotive forces on the loop antenna potential is estimated theoretically.

K e y w o r d s: stellarator, torsatron, high-frequency heating, escaping electrons.

1. Introduction

In the Uragan-2M (U-2M) stellarator [1, 2], plasma is created and heated by applying radiofrequency (RF) methods in the ion-cyclotron frequency interval (3–15 MHz) [3, 4]. One of the main differences distinguishing RF methods of plasma heating from the others is the formation of spatial charges composed of positive ions in the near-antenna region. It is known that, if RF plasma heating methods are used, the parallel electric field creates spatial RF layers near the RF antenna surface. These layers favor the formation of convective cells, the formation of additional impurities because of the antenna material sputtering, and the power dissipation at the plasma cord boundary [5, 6]. Such layers have been known for a long time; sometimes, when the matter concerns antennas, they are called near-field RF layers. The location of such layers can be determined by the positions of the magnetic field line and the antenna. The potential of the RF layer with respect to the installation housing depends on the current strength in the antenna, i.e., it is determined by the level of the RF power introduced into the antenna [7]. High quasi-stationary electric fields were discovered as long ago as in the 1930s, when the parameters of the plasma created by the RF method were measured using the probe method. The intensity of such fields can reach units and tens of kilovolts per centimeter. The measurement results showed that the potential difference between the plasma and the electrodes can reach values that by the order of magnitude are equal to the voltage applied to the electrodes [5, 8, 9].

Similar layers in plasma were also studied in works [10, 11] The occurrence of substantial poten-

C i t a t i o n: Korovin V.B., Tarasov I.K., Leleko Ya.F., Sorokovyi E.L., Kovtun Yu.V., Shapoval O.M., Kozulya M.M., Lozin O.A., Tarasov A.M., Krams'kyi E.D., Filippov V.V., Yevsyukov O.V. Dynamics of the ungrounded antenna potential in an Uragan-2M torsatron during an RF pulse. *Ukr. J. Phys.* **70**, No. 3, 178 (2025). https://doi.org/10.15407/ujpe70.3.178.

tial changes near the RF antenna was discussed in work [12]. In work [13], data on the measurements of the plasma potential were presented, which also confirmed the presence of a layer near the antenna, if the RF power is applied. As a rule, the spatial layer consists of several sublayers [14]. This occurs due to the effect of RF voltage rectifying by the near-electrode space charge layer [15]. The resulting space charge layers have a pronounced nonlinear current-voltage characteristic [16]. If electrons escaping from the near-antenna region fall on the antenna surface, the antenna acquires a negative charge. Actually, this is the beginning of the space charge formation. In turn, the plasma becomes positively charged with respect to the antenna. We may say that a capacitance is formed between the antenna and the plasma. The formation of such a capacitance leads to the appearance of a capacitive connection between the antenna and the plasma, thus creating an additional channel for the RF energy input into the plasma. That is, there emerges a hybrid (inductive-capacitive) discharge [17–19]. As a result, the RF power can enter the plasma through both discharge channels, inductive, and capacitive. At the same time, the plasma remains quasi-neutral beyond this space charge layer [20].

In the U-2M stellarator, the formation of a spatial layer is also observed in the near-antenna region, where a plasma capacitor between the RF antenna surface and the plasma is also formed. This mechanism was described in work [13].

The presence of high-voltage space charge layers negatively affects the surface of RF antennas. The antenna material is sputtered, which leads to the appearance of heavy impurities in the plasma [18, 21]. As a result, the concentration and temperature of electrons in the peripheral plasma change. These effects can lead to plasma degradation in the plasma confinement volume [6, 16]. For the U-2M stellarator, this problem is all the more important because of the absence of a diverter that could output the results of the peripheral plasma layer interaction with the chamber wall and the antenna. The problem of the arrival of heavy impurities due to the sputtering of the antenna material during the RF plasma creation is very challenging and needs to be solved. Some possible solutions were given in works [13, 22, 23]. The distribution of the stationary potential can also be affected by ponderomotive forces acting on plasma particles near the antenna in the presence of the RF field [24, 25].

The research of the negative potential dynamics of the loop antenna in the Uragan-3M (U-3M) and U-2M installations allows a broader interpretation of the results previously obtained for the plasma breakdown and retention, as well as the emergence of transport barriers, to be made. For example, these installations were used to carry out experiments [26, 27], where a negative potential was applied to the peripheral region of the plasma cord in order to experimentally confirm the possibility of suppressing the flows of escaping electrons (EEs). The difference between the conditions of the experiments dealing with EE suppression and those with the emergence of a potential as a result of the RF voltage application to the antenna consisted in that the potential was applied continuously in the former case (Uragan-3M [28]), and only during the RF pulse in the latter one (Uragan-2M [29]). In the former case, the EE flux was suppressed at the stage of its formation; in the other one (the antenna potential), this occurred with the already-formed flux of high-energy electrons. For this reason, there were substantial differences between the effects of the antenna's potential influence on electrons. In the former case, a complete suppression was observed (within the accuracy of our measurements). In the latter one, the EE flux strongly interacted with the plasma, the RF fields, and the antenna potential. Moreover, the flux of electrons that lost their speed during the RF pulse could continue ionization after the RF pulse termination. Probably, this effect could take place in the U-3M stellarator [28].

As concerning the study of the antenna's potential influence on the dynamics of created plasma, it should be noted that this topic attracted attention earlier [29, 30], but had no further development.

A direct study of the space charge interaction with the RF antenna surface is complicated owing to the high RF power and voltage at the antennas, as well as small geometric dimensions of the layer itself. Therefore, any new methods aimed at studying the space charge are important for a more complete understanding of the RF antenna interaction with plasma.

The aim of this work was to study the dynamics of the DC voltage between the RF antenna and the installation housing without introducing additional measuring probes into plasma and to obtain the dependence of this voltage on such experimental param-

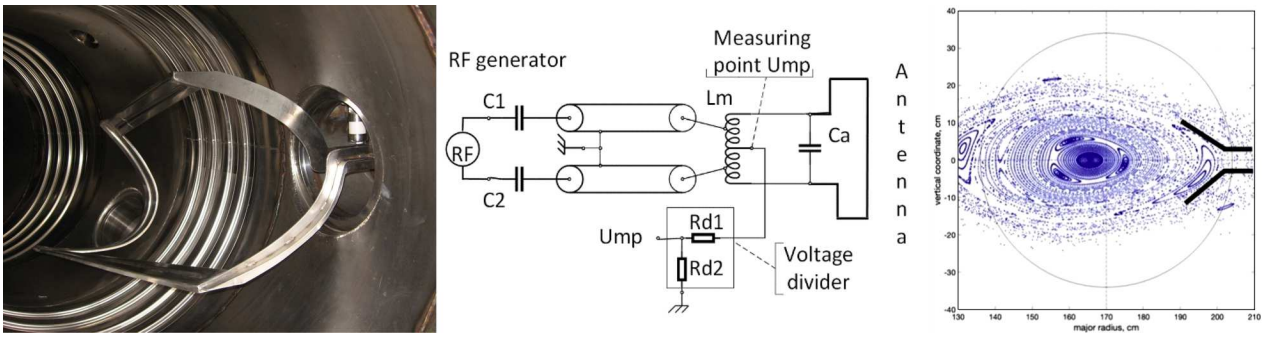

a *b* *c*

Fig. 1. Photo of the loop antenna installed in the Uragan-2M chamber (*a*). Schematic diagram of connecting the RF antenna to the experimental unit for measuring U_{mp} (*b*). Schematic arrangement of the loop antenna with respect to the calculated magnetic surfaces in the installation chamber (*c*)

eters as the RF voltage level at the antenna and the working gas pressure.

The paper structure is as follows. In Section 2, the experimental conditions and measurement procedures are described. The results of experimental measurements are presented in Section 3. Section 4 is devoted to the theoretical analysis of the influence of ponderomotive forces on the DC potential distribution near the antenna. Section 5 contains the conclusions drawn from the performed studies.

2. Experimental Part

The Uragan-2M [1] is a torsatron-type stellarator with the major plasma radius $R = 170$ cm, the average value of minor plasma radius $r_{\rm pl} < 24$ cm, and the toroidal magnetic field $B_0 < 0.4$ T. The minor radius of the vacuum chamber was 34 cm. As was already indicated above, the RF method [31, 32] was used to create and heat the plasma in the U-2M torsatron. The mechanisms of plasma creation and heating in the U-2M were discussed in works [3, 33] in detail.

Various antennas, including ungrounded loop-type ones [33–35], were used. The loop antenna is mainly used in the U-2M for preionization, i.e., for creating cold low-density plasma. The output power of the RF generator to which the antenna was connected was about 50 kW in this case. The loop antenna sizes were 70 cm in the toroidal direction and 50 cm in the poloidal one. The antenna was made of stainless nonmagnetic steel. The shape of its conductors was adjusted to the shape of the last closed magnetic surface of the torsatron. The antenna was located at a distance of 1 cm from the latter (see Figs 1, *a* and *c*). The loop antenna was located outside of the plasma cord at a place, where the elliptical cross-section of the cord was oriented horizontally [33].

The loop antenna was electrically disconnected from the installation housing; it had a bipolar input, which is well suited for connecting the output of a push-pull RF generator Kaskad. RF generators Kaskad-1 and Kaskad-2 were the sources of the RF electromagnetic field used to create plasma [1, 36]. These were powerful pulse devices made according to the scheme of a push-pull self-excited oscillator with a common cathode [37].

When operating with a symmetrical load (the loop antenna), the RF voltage was 0 V at its midpoint (provided the balanced generator arms). That is, during the RF pulse of generator, the RF voltage was practically not observed at this point, which was convenient when measuring the DC voltage.

When studying the plasma generation mode using the loop antenna in the U-2M torsatron, the voltage U_{mp} at the midpoint of the matching device was monitored (this midpoint is the equipotential midpoint of the ungrounded loop antenna [38]). Figure 1, *b* demonstrates the schematic diagram of measurements. Here, C_1 and C_2 are the blocking capacitors at the RF generator output, C_a is the antenna circuit capacitor, and L_m is the inductance of the matching device for the RF antenna, which is installed inside the vacuum chamber. RF voltage measurements were carried out by means of RF capacitive voltage dividers. The voltage U_{mp} was measured using the resistive voltage dividers R_{d1} and R_{d2} with input resistances of 15.1–57.6 kΩ.

The process of RF plasma creation can be divided into three stages, which differ from each other by the electromagnetic field distribution and the character of the ionization process [40]. The first stage is pre-wave (the neutral gas breakdown), when the plasma density is so low that it has little effect on the electromagnetic field structure. The second stage is the stage of preliminary ionization. At this stage, waves can propagate, and the plasma density is low as compared to the neutral gas density. The third stage is the creation of plasma with a high ionization degree [40].

In the case where the plasma is created and heated using the loop antenna, the plasma density increases rather quickly after the RF pulse starts. This occurs because the loop antenna effectively excites a slow wave, so, the two stages of the plasma creation, the pre-wave and pre-ionization ones, last for a short period of time [40, 41].

In this work, we consider the processes that are mainly related to the first stage.

3. Experimental Results

It was found in the course of measurements that during the RF generator operation to create plasma, the DC voltage U_{mp} at the measurement point (see Fig. 1, *b*) has both positive and negative components during the RF pulse period (see Fig. 2). Furthermore, this phenomenon was observed both at low magnetic field values $B_0 = 0.01$ T (in the chamber cleaning mode) and at $B_0 = 0.33$ T.

In work [38], a detailed analysis of why the positive component of the DC voltage appears at the antenna was made. It turned out that the main reason for such an appearance is the circuit and technical features of the RF generator Kaskad, namely, the discharge of the generator's blocking capacitor through the load (plasma) when the generator is being switched on. The cited work also contains the results of the study concerning the dependence of this voltage on the voltage at the anodes of the RF generator's lamps and the working gas pressure in the installation chamber. It was suggested that the elimination of the positive component of the DC voltage at the antenna can contribute to the reduction of the working gas breakdown. A solution was proposed for the elimination of the positive surge of the DC voltage U_{mp} at the beginning of the RF pulse. Therefore, in this work, we consider only the negative component of the antenna potential with respect to the installation housing.

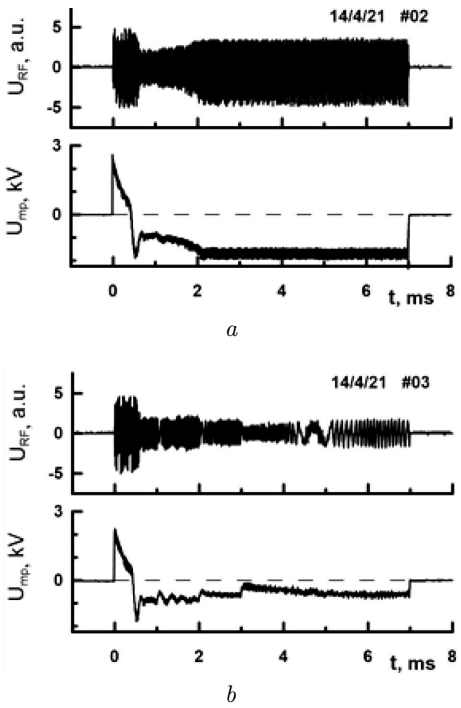

Fig. 2. Time dependences of the RF voltage at the antenna leads (*a*) and the antenna potential U_{mp} (*b*) for $P = 4 \times 10^{-4}$ Torr, $B_0 = 0.01$ T, and the supply voltages of the RF generators (*a*) $U_{K2} = 4$ kV and (*b*) $U_{K2} = 4$ kV (0–7 ms), $U_{K1} = 5$ kV (2–7 ms)

Below, we present the data obtained while studying the dynamics of the negative component of the antenna potential with respect to the installation housing.

The variations of the RF voltage U_{RF} at the loop antenna input and the voltage U_{mp} at the midpoint are plotted in Fig. 2. Panel *a* corresponds to the operating mode when plasma is created using the loop antenna but without its further heating with the help of the second RF generator. The plots for U_{mp} in both panels demonstrate that changes in the DC antenna potential U_{mp} reflect changes in the RF voltage at the antenna.

Approximately 0.5 ms after the RF pulse starts, a sharp decrease in the RF voltage at the antenna takes place. At this stage, the working gas molecules (hydrogens) are ionized by electrons that obtain an energy necessary for hydrogen ionization in the longi-

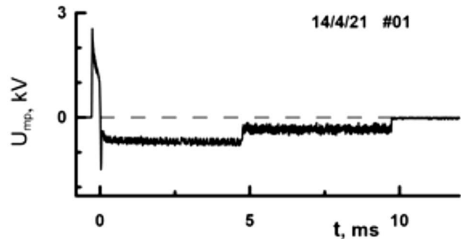

Fig. 3. Dynamics of the antenna potential U_{mp} during the operation of only one or simultaneously two (5–10 ms) RF generators. $U_{K2} = 4$ kV (0–10 ms). $U_{K1} = 5$ kV (5–10 ms). $P = 3 \times 10^{-4}$ Torr (hydrogen). $B_0 = 0.01$ T

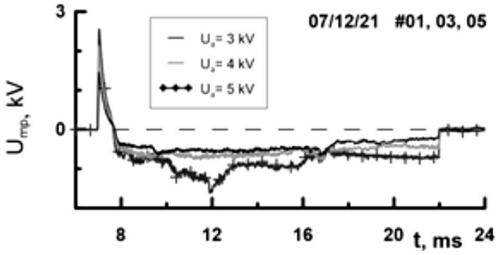

Fig. 4. Dynamics of the antenna potential U_{mp} for various anode voltages of the RF generator. $P = 6.5 \times 10^{-5}$ Torr (hydrogen), $B_0 = 0.33$ T

tudinal RF electric field $E_{||} = \mathbf{E} \cdot \mathbf{B}_0/B_0$ [37]. Since the waves do not propagate in the plasma ($k_\perp r_{\rm pl} < 1$, where $r_{\rm pl}$ is the plasma radius, and $k_\perp$ is the transverse component of the wave vector) at the RF breakdown stage, the RF potential is small everywhere except in the near-antenna region. Therefore, electrons that are born in the near-field antenna region have a substantial oscillation energy, can ionize the neutral gas, and initiate the avalanche breakdown. When the gas becomes ionized, there appears radiation H_α [38]. The emerging plasma introduces its resistance into the antenna circuit and thereby loads the antenna and, accordingly, the RF generator. It was found experimentally that the RF breakdown and the gas reionization occur only at certain values of the antenna RF current [39]. The current in the antenna depends on the voltage at its leads and the resistance of the load introduced by the plasma. The larger the load, the lower the level of U_{mp}. It was observed that the level of the RF voltage after the breakdown gradually increased, that is, the influence of the plasma on the antenna (the load of the RF generator) diminished. The coupling between the antenna and the plasma decreases, and the plasma parameters degrade. This may happen, because more and more plasma electrons fall on the antenna surface; as a result, the U_{mp}-level increases.

The plot of the antenna potential dependence (see Fig. 2, *b*) corresponds to the mode, when, after the initial plasma creation by one of RF generators with the help of the loop antenna, further plasma heating was performed by the second RF generator using another, two-and-a-half-turn antenna [3, 44].

After the breakdown, a certain plateau in the value of U_{mp} is observed. After that, the RF voltage decreases at the 1st, 2nd, and 3rd ms, which is caused by the switching-on of the second RF generator with a stepwise increase of the voltage. This process is accompanied by an analogous drastic stepwise decrease of U_{mp}. In this case, the plasma load on the loop antenna increases [43]. From both plots of the antenna potential dependence (see Figs. 2, *a* and *b*), one can see that the value of U_{mp} is coupled with the RF voltage level.

Figure 3 illustrates a change of U_{mp} in the mode when only one Kaskad-2 generator operates on the loop antenna during the initial 5 ms, and the antenna creates preliminary low-density plasma. The negative potential of the antenna is maximum at that. At the 5th ms, another Kaskad-1 generator is switched on, which is loaded on the two-and-a-half-turn antenna, and the plasma is simultaneously affected by two RF fields from two antennas. As a result, the plasma density increases. Starting from this moment, the DC potential at the antenna first decreases drastically and, afterwards, remains practically unchanged.

In work [42], the value of the loop antenna potential in the U-3M torsatron was reported. If the RF voltage of 2 kV was applied to the antenna, the DC negative potential of the latter reached a value of 1 kV. If the area near the antenna is considered as a near-electrode layer in the case of capacitive RF discharge, then the absolute value of the stationary potential drop in such near-electrode layers can reach a magnitude of the order of the amplitude of the applied RF voltage [5, 15].

We also studied the influence of the voltage at the anodes of the RF generator lamps (see Fig. 4) and the working gas pressure (see Fig. 5) on the changes of the loop antenna potential. Plasma was created by means of an RF generator loaded on the loop antenna within a time interval from 7 to 22 ms. At the 15 ms, the second RF generator loaded on the

two-and-a-half-turn antenna was switched-on, with a stepwise increase of the anode voltage at the generator at the 16 and 17 ms. In both cases, during the first 8 ms, the plasma was affected by the loop antenna only. Afterwards, the RF field from the second antenna (grounded; it continued to operate even after the loop antenna was switched off at the 22 ms) gave its contribution.

As can be seen from the plots in Fig. 4), as the anode voltage increases, the negative antenna potential U_{mp} increases during the entire RF pulse.

From Fig. 5, one can see that the pressure change also affects the magnitude of the negative potential. As the working gas pressure increases, the number of active electrons falling on the antenna surface increases. This circumstance leads to the growth of the negative DC voltage at the antenna.

In Figs. 6 and 7, it is clearly seen that the emission of the H_β line appears at the time moment t_1, when the antenna already possesses the negative potential U_{mp}. The further change of its value depends on the pressure. At the point t_2, the negative amplitude U_{mp} has an extremum. At the time t_3, there appears the emission line CIII of carbon, and the intensity of H_β radiation reaches its maximum.

Immediately before the appearance of the emission line of the CIII ion (at 229.7 nm), the largest negative peaks of the antenna potential were observed (at the point t_2). One can also see that such negative potential peaks (the point t_2 in the plots) were registered at the moment, when the rate of the radiation intensity H_β growth was maximum, and they practically coincide with the moment of the CIII radiation signal appearance.

To achieve a breakdown in the neutral gas, it is necessary to have a longitudinal (along magnetic lines) electric component in the structure of the RF field emitted by the antenna because it induces stronger electronic oscillations than other components of the RF field do. At the same time, the magnitude of this component is maximum in the near-antenna zone. This fact means that the breakdown is initiated near the antenna, so some of the emerging high-energy electrons fall onto the antenna surface.

In Fig. 8, the implementation of the RF breakdown scenario at an elevated pressure is depicted. During the RF pulse of the loop antenna, the voltage U_{mp} was practically constant and reached its negative maximum value even before the appearance of the signal

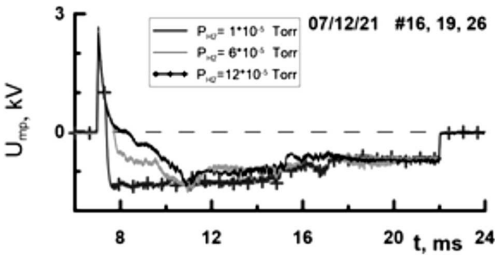

Fig. 5. Dynamics of the antenna potential U_{mp} for various hydrogen pressure values. $B_0 = 0.33$ T, $U_{K2} = 5$ kV

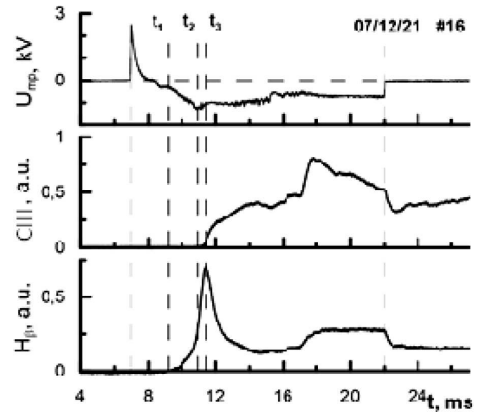

Fig. 6. Time dependences of the DC voltage at the antenna U_{mp}, the intensity of carbon line CIII (229.7 nm), and the intensity of line H_β at $B_0 = 0.33$ T and $P = 1 \times 10^{-5}$

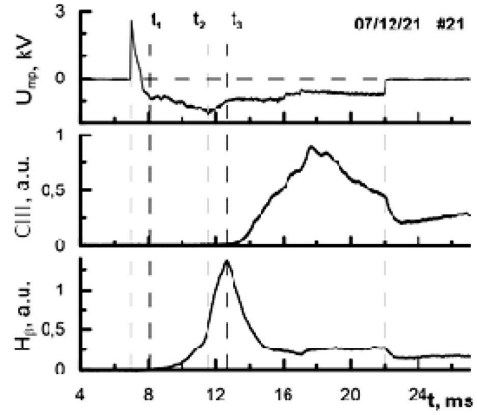

Fig. 7. The same as in Fig. 6, but for $P = 8 \times 10^{-5}$ Torr

H_β, whereas the RF breakdown (t_2, t_3) occurred already during the operation of the second RF antenna (two-and-a-half-turn). In this case, the maximum intensity of the H_β radiation was also registered in all experiments with this series of pulses. This is a regime of weakly ionized plasma at elevated pressures, when the RF breakdown is initiated gradually near the an-

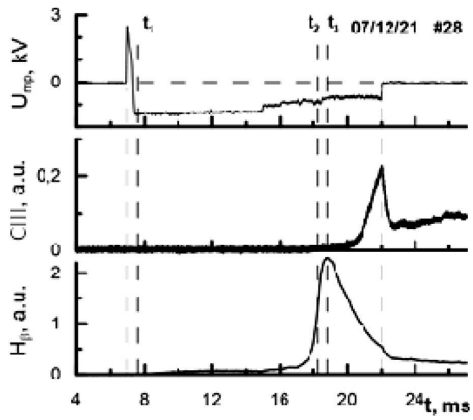

Fig. 8. The same as in Fig. 6, but for $P = 1.7 \times 10^{-4}$ Torr

tenna surface. As a result, the number of electrons falling onto its surface is maximum. At the same time, as was in the cases presented in Figs. 6 and 7, the level of the negative DC voltage at the antenna before the appearance of the H_β radiation was two to three times lower than its maximum value in the same discharge.

When analyzing the dependence of the peak value of the negative antenna potential during the RF pulse on the pressure, one can see that its value increases together with the pressure growth and reaches its absolute maximum at a pressure of 1×10^{-4} Torr.

4. Theoretical Consideration of the Influence of Ponderomotive Forces on the Loop Antenna Potential

The purpose of this theoretical study is to assess the influence of ponderomotive forces on the antenna DC potential and determine its part that can be associated with ponderomotive effects at any time moment. As was mentioned above, in the U-2M, an unscreened loop antenna is used to create and heat hydrogen plasma by means of RF fields in the Alfvén frequency interval $\omega \lesssim \omega_{ci}$ (here, ω is the RF generator frequency, $\omega_{ci} = eB_0/(m_i c)$ is the ion cyclotron frequency, e is the elementary charge, B_0 is the external magnetic field, m_i is the ion mass, and c is the speed of light). The antenna's conductors, which are oriented along the magnetic field, excite a slow magnetoacoustic wave (see Figs. 1, *a* and 1, *c*). The calculated generation maximum is located at the toroidal wave number $l = 11$ [45]. At the same time, conductors oriented in the poloidal direction excite mainly a fast magnetoacoustic wave. In this case, the generation maximum is located at $l = 8 \div 11.26$ [45].

The following parameter values were used for the estimation: $B_0 = 7$ kG, the electron concentration $n_e = 10^{10}$ cm^{-3}, the electron temperature $T_e = 50$ eV, the ion temperature $T_i = 10$ eV, $\omega = 5.5 \times 10^7$ s^{-1}, and $l = 10$. These values may be relevant in future experiments.

A Cartesian coordinate system was used for the calculations, with the z-axis being directed along the magnetic field lines, the y-axis along the antenna conductors, which are perpendicular to the magnetic field, and the z-axis perpendicularly to the antenna plane (the antenna is assumed to be flat). As is known, plasma particles of type α moving near a source of electromagnetic radiation in a magnetic field $\omega_{c\alpha} \gtrsim \omega$, $\omega_{c\alpha}$ is the cyclotron frequency of the particles of type α) along the magnetic field lines (the z-direction) are subjected to the action of the ponderomotive force [24, 25, 46]

$$F_{z\alpha} = -\frac{e_\alpha^2}{4m_\alpha\omega^2}\frac{\partial}{\partial z}E_z E_z^* + \frac{e_\alpha^2}{4m_\alpha(\omega_{c\alpha}^2-\omega^2)} \times$$
$$\times \frac{\partial}{\partial z}\left\{E_x E_x^* + E_y E_y^* - 2\frac{\omega_{c\alpha}}{\omega}\mathrm{Re}(iE_x E_y^*)\right\}, \quad (1)$$

where $E_{x,y,z}$ are the amplitudes of the electric RF field components near the radiation source, and e_α and m_α are the charge and mass, respectively, of the particles of type α. Expression (1) can be rewritten in the form

$$F_{z\alpha} = \frac{-\partial}{\partial z}\Psi_\alpha, \quad (2)$$

where

$$\Psi_{z\alpha} = -\frac{e_\alpha^2}{4m_\alpha\omega^2}E_z E_z^* + \frac{e_\alpha^2}{4m_\alpha(\omega_{c\alpha}^2-\omega^2)} \times$$
$$\times \left\{E_x E_x^* + E_y E_y^* - 2\frac{\omega_{c\alpha}}{\omega}\mathrm{Re}(iE_x E_y^*)\right\} \quad (3)$$

is the ponderomotive potential acting on the particles of type α.

Let us calculate the ponderomotive potential at the conductors of the loop antenna that are longitudinal or transverse with respect to the external magnetic field. Using the dispersion equation [47]

$$\left(N^2\delta_{ij} - N_i N_j - \varepsilon_{ij}\right)E_j = 0, \quad (4)$$

we find the following relationships between the electromagnetic field components:

$$\frac{E_x}{\Delta_x} = \frac{E_y}{\Delta_y} = \frac{E_z}{\Delta_z}, \quad (5)$$

where

$$\Delta_x = (N^2 - \varepsilon_3)N_x N_y + i\varepsilon_2(N_x^2 + N_y^2), \tag{6}$$

$$\Delta_y = N^2 N_y^2 - \varepsilon_3(N_z^2 + N_y^2) - \varepsilon_1(N_x^2 + N_y^2), \tag{7}$$

$$\Delta_z = ((N^2 - \varepsilon_1)N_y + i\varepsilon_2 N_x)N_z, \tag{8}$$

ε_{ij} is the plasma permittivity tensor with the components ε_1, ε_2, and ε_3; N is the wave refractive index, and $N_{x,y,z}$ are its corresponding components, and δ_{ij} is the Kronecker symbol. In the general case, the expressions for the components of the plasma permittivity tensor look like

$$\varepsilon_1 = 1 + \frac{\omega_{pi}^2}{\omega_{ci}^2 - \omega^2}, \quad \varepsilon_2 = \frac{\omega_{pi}^2 \omega}{\omega_{ci}(\omega_{ci}^2 - \omega^2)},$$

$$\varepsilon_3 = 1 + \frac{\omega_{pe}^2}{k_\parallel^2 v_{Te}^2}\left(1 + i\sqrt{\pi} z_e W(z_e)\right),$$

where

$$W(z_e) = e^{-z_e^2}\left(1 + \frac{2i}{\sqrt{\pi}}\int\limits_0^{z_e} e^{t^2} dt\right), \quad z_e = \frac{\omega}{k_\parallel v_{Te}}.$$

For a fast wave excited by the transverse conductors, in the case $N_y = 0$, we have

$$\frac{E_x}{E_y} = \frac{\Delta_x}{\Delta_y} = \frac{-i\varepsilon_2(\varepsilon_3 - N_x^2)}{(\varepsilon_1 - N_z^2)(\varepsilon_3 - N_x^2) - N_x^2 N_z^2}, \tag{9}$$

$$\frac{E_z}{E_y} = \frac{\Delta_z}{\Delta_y} = \frac{i\varepsilon_2 N_x N_z}{(\varepsilon_1 - N_z^2)(\varepsilon_3 - N_x^2) - N_x^2 N_z^2}, \tag{10}$$

where $N_z = lc/(R_0\omega)$, and N_x is one of the roots of the dispersion equation [47]

$$\varepsilon_1 N_x^4 + \left[\left(N_z^2 - \varepsilon_1\right)(\varepsilon_1 + \varepsilon_3) + \varepsilon_2^2\right] N_x^2 + \\ + \varepsilon_3\left[\left(N_z^2 - \varepsilon_1\right)^2 - \varepsilon_2^2\right], \tag{11}$$

which is approximately given by the expression

$$N_{\perp F}^2 \approx \frac{\left(\varepsilon_1 - N_\parallel^2\right)^2 - \varepsilon_2^2}{\varepsilon_1 - N_\parallel^2}. \tag{12}$$

Figure 9 illustrates the dependences of the amplitude ratios between the electric field components of the fast wave on the magnetic field strength near the region of ion cyclotron resonance ($B_{ci} = 0.81575B_0$) for the $n = 10^{10}$ cm^{-3} and $l = 10$ within an interval of $0.814 \le B/B_0 \le 0.819$; the same scaled-up dependences within an interval of $0.8 \le B/B_0 \le 1.05$ are plotted in Fig. 10. Near the resonance, the x- and z-components of the electric RF field are of the order of the y-component, being much smaller far from the resonance. In Fig. 10, the dependences of $\mathrm{Re}(E_x/E_y) \approx 0$ and $\mathrm{Im}\,(E_z/E_y) \approx 0$ are visible as a single line.

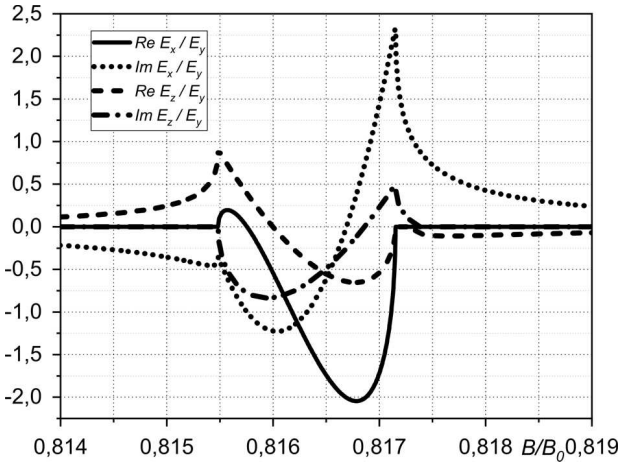

Fig. 9. Dependences of the amplitude ratios between the electric field components of the fast wave on the magnetic field strength in the interval near the ion cyclotron resonance value $B_{ci} = 0.81575B_0$ for $n = 10^{10}$ cm^{-3} and $l = 10$

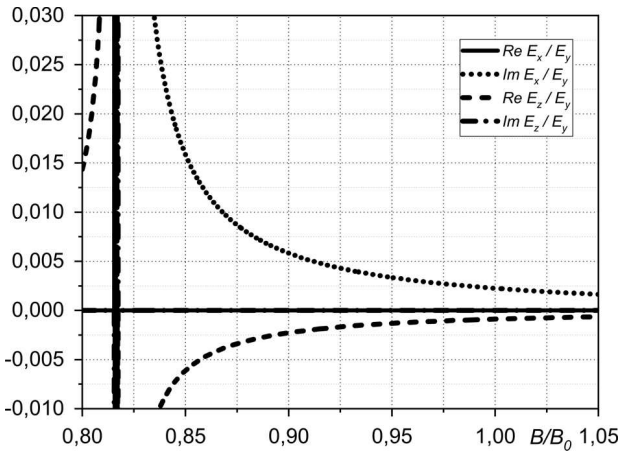

Fig. 10. Scaled-up version of Fig. 9

Figure 11 demonstrates the dependences of the ponderomotive potential, which is excited by the fast wave and acts on ions and electrons, on the mag-

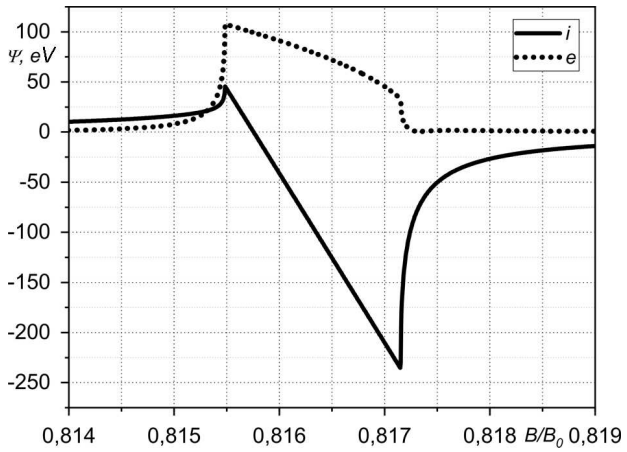

Fig. 11. Dependences of the ponderomotive potential excited by the fast wave on the magnetic field strength in the interval near the ion cyclotron resonance value $B_{ci} = 0.81575B_0$ for $E_y = 30$ V, $n = 10^{10}$ cm^{-3}, and $l = 10$

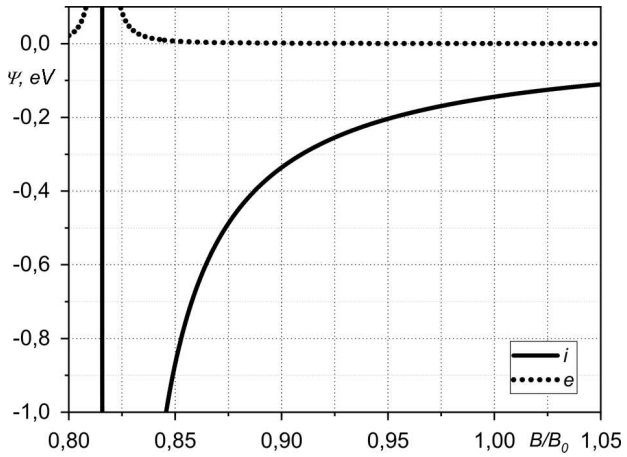

Fig. 12. Scaled-up version of Fig. 11

netic field in the interval near the ion cyclotron resonance region ($B_{ci} = 0.81575B_0$) for $E_y = 30$ V, $n = 10^{10}$ cm^{-3}, and $l = 10$; the same scaled-up dependences within an interval of $0.8 \leq B/B_0 \leq 1.05$ are plotted in Fig. 12. The electric field magnitude was estimated using the relationship $E_y = U_\sim/L$, where $U_\sim$ is the amplitude of the RF voltage applied to the antenna, and L is the total length of the antenna conductors. The specific values are $U_\sim = 7.2$ kV and $L = 240$ cm. Near the resonance, the ponderomotive potential acting on electrons reaches values of about 100 eV, and, in the case of ions, about -200 eV. Furthermore, in the interval $B > B_{ci}$, the ponderomotive potential has different signs when acting on ions and

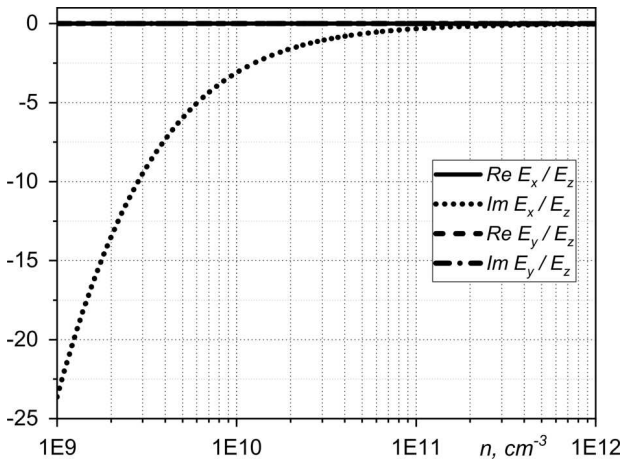

Fig. 13. Dependences of the amplitude ratios between the electric field components of the slow wave on the plasma concentration for $B = B_0$ and $l = 10$

electrons. Far from the resonance, the potential values are small.

For the slow wave excited by the conductors oriented along the magnetic field lines, we obtain, from expressions (5)–(8), the following relationships between the electric RF field components at $N_y = 0$:

$$\frac{E_x}{E_z} = \frac{\Delta_x}{\Delta_z} = \frac{N_x^2 - \varepsilon_3}{N_x N_z}, \tag{13}$$

$$\frac{E_y}{E_z} = \frac{\Delta_y}{\Delta_z} = \frac{(\varepsilon_1 - N_z^2)(\varepsilon_3 - N_x^2) - N_x^2 N_z^2}{i\varepsilon_2 N_x N_z}, \tag{14}$$

where N_x is another root of the dispersion equation (11), which is approximately equals

$$N_{\perp S}^2 \approx -\frac{\varepsilon_3}{\varepsilon_1}\left(N_\parallel^2 - \varepsilon_1\right). \tag{15}$$

In Fig. 13, the dependences of the amplitude ratios between the electric field components of the slow wave on the plasma concentration are shown for the case $B = B_0$ and $l = 10$. The choice of the dependence is determined by the fact that for the longitudinal conductors, which are directed almost along the magnetic field lines, the magnetic field changes slightly, unlike the transverse conductors, which are almost perpendicular to the magnetic field lines. The imaginary part of the x-component of the electric field increases with the decreasing plasma density and becomes much larger than the longitudinal component at $n = 10^{10}$ cm^{-3}. The other three components can

be neglected: they are small and merge into a single line in the plot.

In Fig. 14, the dependences of the ponderomotive potential, which is excited by the slow wave and acts on ions and electrons, on the plasma concentration are shown for the case $B = B_0$ and $l = 10$. The magnitude of the ponderomotive potential, which acts on electrons, does not depend on the plasma concentration and turns out to be equal to about 130 eV. This is a result of the fact that the main contribution to the electronic ponderomotive potential is made by the first term in Eq. (3), which does not depend on the plasma concentration. For electrons, the second term is approximately proportional to $\omega/\omega_{ce} \ll 1$, being comparable with the first one. The ionic ponderomotive potential becomes noticeable at $n = 10^{10}$ cm^{-3} and decreases to about -80 eV at $n = 10^9$ cm^{-3}. In the case of ions, the main contribution is made by the second term in Eq. (3). It increases with the increasing x-component of the electric field, whereas the first term is small because it is of an order of m_e/m_i with respect to the first, electron, term.

For a qualitative explanation of the influence of ponderomotive forces on the plasma parameters in the space charge layer near the antenna, let us use stationary hydrodynamic equations. The equation of motion for electrons, if we neglect the components that are proportional to m_e/m_i, takes the form

$$0 = e\frac{\partial}{\partial z}\varphi - \frac{T_e}{n_e}\frac{\partial}{\partial z}n_e - \frac{\partial}{\partial z}\Psi_e. \tag{16}$$

where φ is the electric potential. After integration, we obtain the Boltzmann formula that takes into account the ponderomotive potential,

$$n_e = n_{e0}\exp\left(\frac{e\varphi - \Psi_e}{T_e}\right). \tag{17}$$

As is known [48], in the stationary case and, in the absence of RF field, the plasma volume can be divided into a transition layer and a quasi-neutrality region. In the case when the penetration depth of the RF field into the plasma is much larger than the Debye–Hückel electron radius $r_{De} = \sqrt{T_e/(4\pi e^2 n_e)}$, the action of the electron ponderomotive potential extends into the quasi-neutrality region, where $n_e \approx n_i$. As can be seen from Eq. (17), the ponderomotive potential Ψ_e acts on electrons as a negative electric potential φ, i.e., it reduces the electron concentration

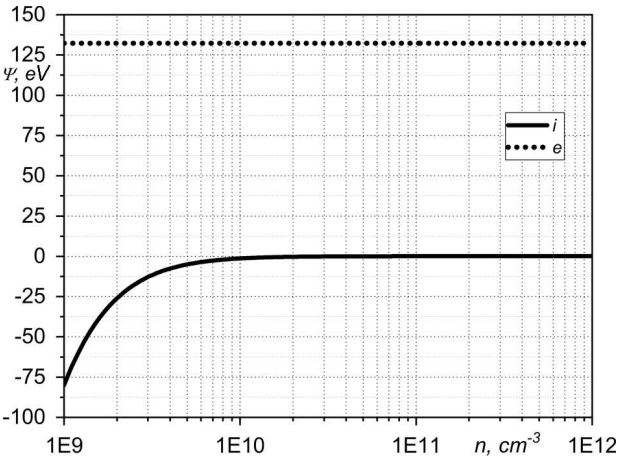

Fig. 14. Dependences of the ponderomotive potential excited by the slow wave on the plasma concentration for $B = B_0$ and $l = 10$

n_e when approaching the antenna, which is simultaneously a source of the RF field. In this case, due to the conservation law of momentum or the continuity equation, the hydrodynamic velocity of ions increases, and the ions reach the velocity of ion sound earlier than in the absence of the RF field, i.e., the size of the transition layer also increases. Similar considerations can be made for the ions. In the transition layer near the antenna, by neglecting the effects of ionization, the charge transfer, and the ion density gradient, from the equation of motion for the ions,

$$m_i v_i \frac{dv_i}{dx} = -e\frac{d\varphi}{dx} - \frac{\partial}{\partial x}\Psi_i, \tag{18}$$

we obtain the following expression for the ion energy:

$$\varepsilon_i = \frac{m_i v_i^2}{2} + e\varphi + \Psi_i. \tag{19}$$

Since the hydrodynamic flow of ions $j_i = n_i v_i \approx$ const in the transition layer, then

$$n_i \sim (\varepsilon_i - e\varphi - \Psi_i)^{-1/2}. \tag{20}$$

Whence it follows that the negative ion ponderomotive potential Ψ_i has the same effect on the plasma ions as the negative electric potential φ has, i.e., it reduces the ion concentration n_i. If we assume the electron and ion concentrations in formulas (17) and (20) to be constant, then the positive electron, Ψ_e, and the negative ion, Ψ_i, ponderomotive potentials diminish the absolute value of the electric potential $|\varphi|$.

When plasma particles, the antenna surface, and the RF field interact, a rectified potential appears on the antenna. The value of the constant potential measured in the experiments is the sum of the potential of the isolated probe and this rectified potential [10]. As can be seen from Fig. 11, the ratio between the measured DC potential U_{mp} to the amplitude of the applied RF voltage $U_{\sim}$ equals $U_{mp}/U_{\sim} \approx 0.2$. In the case $U_{\sim} = 7.2$ kV, the value of the measured DC potential equals $U_{mp} \approx 1.5$ kV.

The performed estimates show that for the fast wave, which is excited by the antenna conductors oriented transversely to the external magnetic field lines, a substantial increase in the ponderomotive potential is observed in the region near the ion cyclotron resonance ($B \approx B_{ci}$). In this region, the contribution of the ponderomotive potentials of electrons and ions to the measured DC potential of the antenna reaches the values $|\Psi_{e,i}/(eU_{mp})| \approx 7 \div 15\%$ for the plasma parameters that were indicated above. Beyond the resonance, the ponderomotive potential values are small for both electrons and ions. For the slow wave, which is excited by the antenna conductors oriented longitudinally to the external magnetic field lines, the contribution of the ponderomotive potentials of electrons and ions to the measured DC potential of the antenna reaches the values $|\Psi_{e,i}/(eU_{mp})| \approx 5 \div 10\%$ for the plasma parameters indicated above.

Here, in order to scale the results obtained while calculating the influence of the ponderomotive potential, we used the value of the AC voltage U of the generator that was larger than that in the experiment.

When the amplitude of the voltage applied to the antenna decreases, the percentage contribution of the ponderomotive potentials also decreases, $\Psi_{e,i}U^2$ but $U_{mp}U$. Therefore, for the RF generator voltage value $U = 4.5$ kV, which was used in the experiment, the contribution of the ponderomotive potentials of electrons and ions to the measured DC potential of the antenna equals $|\Psi_{e,i}/(eU_{mp})| \approx 5 \div 10\%$ provided the same conditions as in the case with $U = 7.2$ kV.

The calculation of the spatial and temporal distributions of the ponderomotive potential near the antenna may become the subject of further research.

5. Conclusions

To summarize the results of the performed research, it is shown that, during the operation of the Kaskad RF generator for the creation of plasma in the Uragan-2M torsatron, the DC voltage of the loop antenna U_{mp} measured at the midpoint of the device that matches the output impedance of the generator with the plasma load in the antenna has both a positive and negative components during the RF pulse, which allows us to speak about the presence of a space charge near the antenna surface.

It is found that the magnitude of the negative potential U_{mp} depends on the voltage at the anodes of the RF generator lamps: as the latter increases, U_{mp} also increases by absolute value. The value of $|U_{mp}|$ also increases together with the growth of the working gas pressure in the installation chamber.

The magnitude of the negative potential of the loop antenna is measured. It fluctuated within an interval of $1 \div 1.7$ kV. The maximum value of U_{mp} recorded in the experiments, was –1.75 kV. It is registered at the moment, when the rate of the radiation signal H_β growth was maximum.

Our calculations showed that, at the external magnetic fields B near the ion cyclotron resonance ($B \approx \approx B_{ci}$), the contribution of the ponderomotive potentials of electrons and ions near the antenna conductors oriented transversely and longitudinally to the external magnetic field reaches values of $7 \div 15\%$ for the indicated plasma parameters. Taking the positive electron and negative ion ponderomotive potentials into account leads to a reduction in the concentrations of ions and electrons, and a reduction of the electric potential by its absolute value.

In the future, we plan to carry out similar studies for the two-and-a-half-turn W7-X-shaped antenna in Uragan-2M.

The authors thank Rostyslav Pavlichenko for information concerning the arrangement of magnetic surfaces in the Uragan-2M installation.

V.B. Korovin was partially sponsored by Simons Foundation Grant (No. 1290591).

1. O.S. Pavlichenko and for the U-2M group. First results from the URAGAN-2M torsatron. *Plasma Phys. Control. Fusion* **35**, B223 (1993).
2. V.E. Bykov, A.V. Georgievskij, V.V. Demchenko, Yu.K. Kuznetsov, Yu.A. Litvinenko, A.V. Longinov, O.S. Pavlichenko, V.A. Rudakov, K.N. Stepanov, V.T. Tolok. Uragan-2M: A torsatron with an additional toroidal field. *Fusion Techn.* **17**, 140 (1990).
3. V. Moiseenko *et al.* First experiments on ICRF discharge generation by a W7-X-like antenna in the Uragan-2M stellarator. *J. Plasma Phys.* **86**, 905860517 (2020).

4. M.D. Carter, A.I. Lysojvan, V.E. Moiseenko, N.I. Nazarov, O.M. Shvets, K.N. Stepanov. Plasma production using radiofrequency fields near or below the ion cyclotron range of frequencies. *Nucl. Fusion* **30**, 723 (1990).
5. S.M. Levitsky. The space potential and electrode sputtering in the RF discharge. *Zh. Tekhn. Fiz.* **27**, 1001 (1957) (in Russian).
6. I.R. Myra, D.A. D'Ippolito, D.A. Russel *et al.* Nonlinear ICRF plasma interactions. *Nucl. Fusion* **46**, S455 (2006).
7. C.E. Thomas *et al.* ICRF/edge interaction guidelines for ICRF antenna design and initial ICRF/edge interaction experiments on the Tore Supra Tokamak. *Fusion Tech.* **30**, 1 (1996).
8. D. Banerji, R. Ganguli. On deposits of metallic mercury by high-frequency discharge. *Phil. Mag.* **15**, 678 (1933).
9. D. Banerji, R. Ganguli. On the distribution of space-potential in high-frequency glow discharge. *Phil. Mag.* **11**, 410 (1931).
10. V.A. Godyak, A.A. Kuzovnikov. About valve properties of RF-discharge. *Plasma Phys. Rep.* **1**, 496 (1975).
11. V.A. Godyak, A.N. Ivanov, A.A. Kuzovnikov. Changes of Langmuir probe floating potential by the alternating voltage. *J. Tech. Phys.* **37**, 1063 (1967).
12. Ya.F. Leleko, L.I. Grigor'eva, V.V. Chechkin, D.L. Grekov. Influence of the loop-type antenna on the RF-discharge peripheral plasma parameters in the Uragan-3M torsatron. *Probl. At. Sci. Technol. Ser. Plasma Phys.* **107**, 40 (2017).
13. S.J. Wukitch, B. LaBombard, Y. Lin, B. Lipschultz, E. Marmar, M.L. Reinke, D.G. Whyte, and the Alcator C-Mod Team. ICRF specific impurity sources and plasma sheaths in Alcator C-Mod. *J. Nucl. Mater.* **390–391**, 951 (2009).
14. V.A. Godyak. A stationary low-pressure RF discharge. *Fiz. Plazmy* **2**, 141 (1976).
15. V.A. Godyak, A.A. Kuzovnikov. On valve properties of RF discharges. *Plasma Phys.* **1**, 496 (1975).
16. V.L. Berezhnyj. ICRF-volume charge-antenna edge interactions in the U-3M and U-2M torsatrons. Part 3. ICRF – VSC interaction. *Probl. At. Sci. Technol. Ser. Plasma Phys.* **117**, 10 (2017).
17. Yu.P. Raiser, M.N. Schneider, N.A. Yatsenko *High-Frequency Capacitive Discharge: Physics. Experimental Technique. Applications* (Nauka, 1995) (in Russian).
18. M.L. Mayoral, P.U. Lamalle, D. van Eeser *et al.* Hydrogen plasmas with ICRF inverted minority and mode conversion heating regimes in the JET tokamak. *Nucl. Fusion* **46**, 550 (2006).
19. K.V. Vavilin, M.A. Gomorev, E.A. Kralkina, P.A. Neklyudova, V.B. Pavlov, Chen Zhao. Experimental study of plasma parameters of low-pressure hybrid RF discharge. *Vestn. Mosk. Univ. Ser. 3 Phys. Astronom.* No. 1, 101 (2012) (in Russian).
20. E.P. Velikhov, A.S. Kovalyov, A.T. Rakhimov. *Physical Phenomena in the Gas-Discharge Plasma* (Nauka, 1987) (in Russian).
21. E.D. Volkov, L.I. Grigor'eva, Yu.G. Zaleskij, V.G. Konovalov, N.I. Nazarov, I.I. Patlaj, G.N. Polyakova, A.I. Skibenko, A.S. Slavnyj, V.V. Chechkin, A.N. Shapoval. On the mechanisms of light and heavy impurity release during RF plasma heating in the Uragan-3 Torsatron. *Fusion Engineering and Design* **12** (1–2), 237 (1990).
22. Vl.V. Bobkov, R. Bilato, F. Braun *et al.* ICRF antenna coupling dependence on edge plasma conditions in ASDEX Upgrade. *Nucl. Fusion* **46**, 469 (2006).
23. D.A. D'Ippolito, I.R. Myra, J.H. Rogers *et al.* Analysis of RF sheath interactions in TFTR. *Nucl. Fusion* **38**, 1543 (1998).
24. R. Klima. On the motion of particles in nonresonant RF and magnetostatic fields. *Czech. J. Phys.* **16**, 681 (1966).
25. R. Klima. The drifts and hydrodynamics of particles in a field with a high-frequency component. *Czech. J. Phys.* **18**, 1280 (1968).
26. V.E. Moiseenko, V.B. Korovin, I.K. Tarasov *et al.* The effect of an electrostatic field on runaway electrons in the Uragan-3M stellarator. *Techn. Phys. Lett.* **40**, 669 (2014).
27. V.B. Korovin, I.K. Tarasov, E.D. Kramskoi, D.A. Sitnikov, N.B. Dreval', A.V. Lozin, M.M. Kozulya. Suppression of runaway electron flows and specific features of working gas breakdown in the Uragan-2M torsatron. *Techn. Phys.* **63**, 960 (2018).
28. V.K. Pashnev, I.K. Tarasov, D.A. Sitnikov, V.N. Bondarenko, V.V. Chechkin, A.N. Shapoval, R.O. Pavlichenko, M.I. Tarasov, E.L. Sorokovoy, A.A. Petrushenya, A.I. Skibenko, L.L. Karpuhin, A.V. Lozin. The problem of plasma density increasing in the U-3M torsatron after RF heating termination. *Vopr. At. Nauki Tekhn.* **83**, 15 (2013) (in Russian).
29. L.I. Grigorieva, B.I. Smerdov, V.V. Chechkin. On the influence of the antenna electrostatic field on the behavior of peripheral plasma during RF heating. Preprint KhPTI 86-13. (KhPTI of the Academy of Sciences of the Ukrainian SSR, 1986).
30. L.I. Grigorieva, A.V. Pashchenko, B.I. Smerdov, V.V. Chechkin Study of the processes of plasma potential formation and particle transport under the influence of an external alternating electric field. Preprint KkPTI 84-8 (TsNIIatominform, 1984).
31. I.M. Pankratov *et al.* Behavior of RF discharge plasmas in the Uragan-3M and Uragan-2M torsatrons. *Contrib. Plasma Phys.* **50**, 520 (2010).
32. A.G. Dikiy, S.S. Kalinichenko, A.A. Kalmykov *et al. Plasma Phys.* **18**, 557 (1976).
33. V.E. Moiseenko, A.V. Lozin, M.M. Kozulia, Yu.K. Mironov, V.S. Romanov, V.G. Konovalov, A.N. Shapoval. Alfven plasma heating in stellarator URAGAN-2M. *Ukr. J. Phys.* **62**, 311 (2017).
34. V.E. Moiseenko *et al.* RF plasma production and heating below ion-cyclotron frequencies in Uragan torsatrons. *Nucl. Fusion* **51**, 083036 (2011).
35. V.E. Moiseenko *et al.* Progress in stellarator research at IPP-Kharkov. *Nukleonika* **61**, 91 (2016).

36. V.B. Korovin, E.D. Kramskoy. Radio-frequency equipment for Uragan stellarators. *Probl. At. Sci. Technol. Ser. Plasma Phys.* **6**, 19 (2012).
37. M.S. Neiman. *Course Of Radio Transmitting Devices.* (Sovetskoe radio, 1957) (in Russian).
38. V.B. Korovin, I.K. Tarasov, A.V. Lozin, M.M. Kozulia, E.L. Sorokovoy, E.D. Kramskoy, V.Yu. Gribanov, D.I. Baron, S.A. Tsybenko. Behavior features of the ungrounded antenna potential shift in URAGAN-2M torsatron. *Probl. At. Sci. Technol. Ser. Plasma Phys.* No. 1, 9 (2023).
39. A.I. Lysojvan, V.E. Moiseenko, O.M. Schvets, K.N. Stepanov. Analysis of ICRE ($\omega \leq \omega_{ci}$) plasma production in large scale tokamaks. *Nucl. Fusion* **32**, 1361 (1992).
40. V.E. Moiseenko, Yu.S. Stadnik, A.I. Lysoivan, V.B. Korovin. Self-consistent modeling of radio-frequency plasma generation in stellarators. *Plasma Phys. Rep.* **39**, 873 (2013).
41. V.E. Moiseenko, Yu.S. Stadnik, O.M. Shvets *et al.* RF plasma production in Uragan-2M torsatron. In *Proceedings of the 17th Topical Conference on Radio-Frequency Power in Plasma, Clearwater, Florida, USA* (2007) [ISBN: 9780735404441].
42. Ya.F. Leleko, L.I. Grigor'eva, V.V. Chechkin, D.L. Grekov. Influence of the loop-type antenna on the rf-discharge peripheral plasma parameters in the URAGAN-3M torsatron. *Probl. At. Sci. Technol. Ser. Plasma Phys.* **107**, 40 (2017).
43. V.B. Korovin, V.V. Filippov, M.M. Kozulya *et al.* Effect of plasma on the radio-technical characteristics of the Uragan-2M torsatron matching RF systems. *Probl. At. Sci. Technol. Ser. Plasma Phys.* **94**, 41 (2014).
44. A.V. Lozin, Yu.V. Kovtun, V.E. Moiseenko, S.M. Maznichenko, M.M. Kozulia, V.B. Korovin, A.N. Shapoval, E.D. Kramskoy, R.O. Pavlichenko, N.V. Zamanov, M.M. Makhov, A.Yu. Krasyuk, Y.V. Siusko, A.I. Tymoshenko, V.M. Listopad, T. Wauters, Ye. Kazakov, J. Ongena. Two-strap RF antenna in Uragan-2M stellarator. *Probl. At. Sci. Technol. Ser. Plasma Phys.* **130**, 10 (2020).
45. N.T. Besedin, S.V. Kasilov, I.M. Pankratov, A.I. Pyatak, K.N. Stepanov. In: *Proceedings of the VIII IAEA Stellarator Workshop, Kharkov* (IAEA, 1991), p. 53.
46. R. Klima. Drift approximation for a field with a nonresonant high-frequency component. *J. Exper. Theor. Phys.* **26**, 535 (1968).
47. A.I. Akhiezer, I.A. Akhiezer, R.V. Polovin, A.G. Sitenko, K.N. Stepanov. *Plasma Electrodynamics* (Nauka, 1974) (in Russian).
48. Ya.F. Leleko, D.L. Grekov. Influence of ion viscosity on the distributions of plasma parameters in stationary gas discharge. *Ukr. J. Phys.* **66**, 316 (2021).

Received 19.09.24.
Translated from Ukrainian by O.I. Voitenko

В.Б. Коровін, І.К. Тарасов, Я.Ф. Лелеко,
Е.Л. Сороковий, Ю.В. Ковтун, О.М. Шаповал,
М.М. Козуля, О.А. Лозін, А.М. Тарасов,
Є.Д. Крамський, В.В. Філіппов, О.В. Євсюков

ДИНАМІКА ПОТЕНЦІАЛУ
НЕЗАЗЕМЛЕНОЇ АНТЕНИ В ТОРСАТРОНІ
УРАГАН-2М ПРОТЯГОМ ВЧ ІМПУЛЬСУ

У роботі показано, що рамкова ВЧ антена, за допомогою якої створюється первісна плазма в стелараторі Ураган-2М і яка електрично не з'єднана з корпусом установки, набуває як негативного, так і позитивного потенціалу, протягом ВЧ імпульсу. Проведено вивчення впливу на потенціал антени напруги живлення ВЧ генератора і тиску робочого газу. Показано зміну величини потенціалу антени за одночасної роботи двох ВЧ генераторів. Надано теоретичну оцінку впливу пондеромоторних сил на потенціал рамкової антени.

Ключові слова: стеларатор, торсатрон, високочастотний нагрів, електрони, що втікають.